

SPECTRAL SPARSIFICATION OF LAPLACIAN-CONSTRAINED GAUSSIAN AND HÜSLER–REISS GRAPHICAL MODELS

IGNACIO ECHAVE-SUSTAETA RODRÍGUEZ, AIDA ABIAD, AND FRANK RÖTTGER

ABSTRACT. Graph Laplacians encode graph structures in matrix form, and thus facilitate the application of linear algebra to graph theory. In statistics, two related families of probabilistic graphical models can be parameterized by graph Laplacians. The first one is the Laplacian-constrained Gaussian graphical model (LCGGM), which imposes that the (pseudo-)inverse covariance matrix of a Gaussian random vector is a Laplacian matrix. Applications include graph signal processing and network topology learning. The second one is the Hüsler–Reiss graphical model, which is considered as an extremal analog of the Gaussian graphical model, and can be used in extremal dependence modeling of floods, heatwaves, and financial losses. For both models, the restriction to positive edge weights in the graph Laplacian gives rise to an approach for graph structure learning that does not require tuning parameters. While these approaches yield a strong model fit in many settings, the resulting graph estimates are typically much denser than the underlying ground truth, limiting interpretability and scalability. In order to improve the accuracy of Laplacian-constrained graph learning, we propose to use *spectral graph sparsification* as a post-estimation operation. To do so, we replace the original Laplacian estimate by a sparser Laplacian that is spectrally close, and re-fit the model on the resulting graph. We refer to the two resulting methods as *Spectral-LCGGM* and *Spectral-HR*. We investigate the properties of the proposed estimators and show several theoretical results on their performance. Furthermore, we demonstrate that the newly proposed methods perform well by running simulations on Erdős–Rényi and stochastic block model graphs, and we also showcase their applications to real data.

1. INTRODUCTION

Probabilistic graphical models represent multivariate dependence through graphs, with edges connecting pairs of variables that interact directly after accounting for the others (Lauritzen, 1996). Two recent families of graphical models share the algebraic feature that their precision matrix is a connected weighted graph Laplacian. The first is the *Laplacian-constrained Gaussian graphical model* (LCGGM), that is a degenerate Gaussian supported on the hyperplane $\mathbf{1}^\perp$, in which the Laplacian structure is imposed as a modeling constraint (Egilmez et al., 2017; Ying et al., 2020; Wang et al., 2022; Cai et al., 2023). LCGGMs are widely used in graph signal processing and network topology learning, and are a degenerate-rank counterpart of Gaussian graphical models under multivariate total positivity of order 2 (MTP₂) (Slawski and Hein, 2015; Lauritzen et al., 2019; Wang et al., 2020). The second is the *Hüsler–Reiss graphical model* (HRGM) under *extremal* MTP₂ (EMTP₂) (Engelke and Hitz, 2020; Röttger et al., 2023), which can be considered as an extremal analog of Gaussian graphical models (under MTP₂). Here, the Laplacian structure of the precision characterizes the positivity assumption.

While both models perform well in settings where the graph Laplacian assumption is reasonable, standard estimators return overly dense graphs. In fact, Röttger et al. (2023) show that their estimator for Hüsler–Reiss graphical models under EMTP₂ asymptotically identifies a super-graph of the underlying ground truth. In addition to obscuring model identification, retaining spurious edges in the graph estimates can slow down downstream graph-level computations. Penalized alternatives, for example ℓ_1 - and nonconvex-based formulations for LCGGMs (Ying et al., 2020) or the eglearn

estimator for HRGMs (Engelke et al., 2025), can improve the sparsity of the graph estimates, but may incur a measurable cost in fit quality.

In this paper, we propose to employ techniques from spectral graph theory in order to maintain the fit quality of the unpenalized estimators, while improving upon their sparsity. Our approach is similar to the post-estimation spectral-sparsification approach of Echave-Sustaeta Rodríguez et al. (2026), developed there for the full-rank Gaussian MTP₂ model. Because the precision matrices for LCGGMs and HRGMs are already graph Laplacians, we can apply the deterministic linear-size sparsifier of Batson et al. (2012) (BSS). Our approach is the same in both settings: We learn a dense graph estimate, sparsify the resulting precision matrix, and refit the models on the sparsified support. We call the resulting estimators *Spectral-LCGGM* and *Spectral-HR*, respectively. As a theoretical contribution, we bound the change in log-likelihood induced by the sparsifier in both settings, and establish model-class preservation, together with additional guarantees on variograms and the Hüsler–Reiss exponent measure density (Section 4). The analysis rests on a single identity on $\mathbf{1}^\perp$ that combines a Bregman representation of the log-likelihood gap with the spectral approximation produced by the sparsifier, a degenerate-rank analog of the identity used in Echave-Sustaeta Rodríguez et al. (2026). LCGGM simulations on Erdős–Rényi and stochastic block-model ground truths, and applications of Spectral-HR to extremal Danube river levels and extremal flight delays in the Southern United States show that the sparsifiers retain the log-likelihood of their denser baselines at a significantly reduced edge count, with substantially better graph recovery.

Related work. Spectral sparsification was introduced by Spielman and Teng (2004) and was implemented with various methods in Spielman and Srivastava (2011); Batson et al. (2012); Koutis et al. (2012), being extended to sparsification of strictly diagonally dominant M -matrices via approximate Gaussian elimination (Kyng and Sachdeva, 2016). In statistics and machine learning, these methods have been used for multiple applications, with one of the earliest being Srivastava and Vershynin (2013). One of the closest ideas to ours is Sadhanala et al. (2016), in which these methods are used to sparsify graphs prior to Laplacian-regularized regression while preserving statistical validity. Another application combines ridge spectral sparsification with Laplacian learning for scalable semi-supervised classification (Calandriello et al., 2018). The most direct precedent for the present paper is Echave-Sustaeta Rodríguez et al. (2026), which introduces the post-estimation BSS sparsifier and the Bregman–Loewner analysis for the full-rank Gaussian MTP₂ model. The LCGGM and EMTP₂ Hüsler–Reiss settings in the present paper share the same template but require degenerate-rank versions of the bounds: Kullback–Leibler (KL) divergence on $\mathbf{1}^\perp$, pseudo-determinants, and trace-norm residuals through the projector P . A related LCGGM precedent is Wang et al. (2022), who learn a Laplacian-constrained graph by greedy spectral densification: starting from a sparse base graph, they apply spectral-sparsification-style criteria to incrementally add the most spectrally critical edges. We instead apply sparsification as a post-estimation step with explicit Loewner-order, log-likelihood, and KL guarantees. On the modeling side of LCGGMs, common estimators include the unpenalized CGL of Egilmez et al. (2017), the GLE-ADMM algorithm of Kumar et al. (2020), and the nonconvex NGL-SCAD estimator of Ying et al. (2020). For HRGMs, the canonical dense baseline is the EMTP₂-constrained surrogate maximum likelihood estimator (MLE) (Röttger et al., 2023) and the canonical sparse baseline is the eglearn estimator (Engelke et al., 2025).

2. PRELIMINARIES

2.1. Graphs, Laplacians, and Spectral Sparsification. We consider connected weighted graphs $G = (V, E, c)$ with vertex set V , edge set E , and symmetric weight function $c : V \times V \rightarrow [0, \infty)$. The weighted Laplacian is $L_G := \text{Deg}(G) - A$, where $A = (c_{ij})$ is the adjacency matrix and $\text{Deg}(G) =$

$\text{diag}(k_i)$ the diagonal degree matrix with $k_i = \sum_j c_{ij}$. For a connected weighted graph, L_G is positive semidefinite, satisfies $L_G \mathbf{1} = 0$, and has rank $|V| - 1$.

For $\varepsilon \in (0, 1)$, a graph G' on the same vertex set is an ε -spectral approximation of G if

$$(1) \quad (1 - \varepsilon) z^\top L_G z \leq z^\top L_{G'} z \leq (1 + \varepsilon) z^\top L_G z \quad \forall z \in \mathbb{R}^{|V|}.$$

For symmetric matrices $A, B \in \mathbb{R}^{|V| \times |V|}$ and a subspace $W \subseteq \mathbb{R}^{|V|}$, we write $A \preceq B$ on W if $z^\top A z \leq z^\top B z$ for every $z \in W$. When the suffix “on W ” is omitted, we mean $W = \mathbb{R}^{|V|}$. $A \succeq B$ is defined symmetrically. This is the *Loewner order*, a partial order on symmetric matrices. For Laplacians the natural choice is $W = \mathbf{1}^\perp$, since their kernel $\text{span}(\mathbf{1})$ contributes no information. In this notation, (1) reads $(1 - \varepsilon)L_G \preceq L_{G'} \preceq (1 + \varepsilon)L_G$.

The following deterministic construction, due to [Batson et al. \(2012\)](#), achieves such an approximation with a linear-size number of edges. We use it throughout the paper.

Theorem 2.1. *Let L be a connected weighted Laplacian on d vertices and fix $\eta > 1$. There is a deterministic polynomial-time algorithm that outputs a reweighted subgraph Laplacian \tilde{L} supported on at most $\lceil \eta(d - 1) \rceil$ edges that satisfies*

$$L \preceq \tilde{L} \preceq \kappa(\eta) L \quad \text{on } \mathbf{1}^\perp, \quad \kappa(\eta) := \left(\frac{\sqrt{\eta} + 1}{\sqrt{\eta} - 1} \right)^2.$$

After rescaling \tilde{L} by the constant $2/(1 + \kappa(\eta))$, this becomes the symmetric $(1 \pm \varepsilon)$ Loewner bound $(1 - \varepsilon)L \preceq \tilde{L} \preceq (1 + \varepsilon)L$ on $\mathbf{1}^\perp$ with $\varepsilon = (\kappa(\eta) - 1)/(\kappa(\eta) + 1) = 2\sqrt{\eta}/(\eta + 1)$.

2.2. Laplacian-Constrained Gaussian Graphical Models. A *Laplacian-constrained Gaussian graphical model* (LCGGM) is a centered, degenerate Gaussian random vector X with support $\mathbf{1}^\perp \subset \mathbb{R}^d$, whose precision matrix K is a connected weighted graph Laplacian ([Egilmez et al., 2017](#); [Ying et al., 2020](#); [Wang et al., 2022](#)). The model has a probability density with respect to the Lebesgue measure on $\mathbf{1}^\perp$:

$$(2) \quad f_K(x) = (2\pi)^{-(d-1)/2} \text{Det}(K)^{1/2} \exp\left(-\frac{1}{2} x^\top K x\right), \quad x \in \mathbf{1}^\perp.$$

Here, Det denotes the pseudo-determinant, that is the product of the nonzero eigenvalues. For a sample covariance matrix $S \succeq 0$ obtained from n i.i.d. copies of X , the LCGGM log-likelihood up to additive constants is equal to

$$(3) \quad \ell(K; S) := \log \text{Det}(K) - \text{tr}(KS).$$

This gives rise to the LCGGM-MLE given S

$$(4) \quad \hat{K} = \arg \max_K \ell(K; S) \quad \text{s.t. } K_{ij} \leq 0, \quad \forall i \neq j.$$

As c is restricted to $[0, \infty)$, LCGGM is the Laplacian analog of the Gaussian MTP_2 distributions ([Lauritzen et al., 2019](#); [Wang et al., 2020](#)): both impose nonpositive off-diagonal entries on the precision matrix. However, LCGGM additionally requires zero row sums, so K is the Laplacian of a positively weighted graph.

2.3. Hüsler–Reiss Graphical Models and graph Laplacians. Let $X = (X_1, \dots, X_d)$ be a random vector with continuous marginal cumulative distribution functions F_i . After transforming to exponential margins $X_i^* := -\log(1 - F_i(X_i))$, the threshold-exceedance limit

$$(5) \quad \mathbb{P}(Y \leq y) = \lim_{u \rightarrow \infty} \mathbb{P}(X^* - u\mathbf{1} \leq y \mid \max_{i \in [d]} X_i^* \geq u)$$

yields, under multivariate regular variation, a multivariate (generalized) Pareto vector Y . Assuming asymptotic dependence, Y is supported on $\mathcal{E} := \{y \in \mathbb{R}^d : \max_i y_i > 0\}$ ([Rootzén and Tajvidi, 2006](#); [Hentschel et al., 2025](#)).

A d -variate Hüsler–Reiss distribution is a multivariate Pareto distribution that can be parametrized by a conditionally negative definite variogram matrix

$$\Gamma \in \mathcal{D}^d := \{\Gamma \in \mathbb{R}^{d \times d} : \Gamma = \Gamma^\top, \text{diag}(\Gamma) = 0, x^\top \Gamma x < 0 \forall x \neq 0, x \perp \mathbf{1}\}.$$

Its probability density is proportional to a function λ , typically referred to as exponent measure density:

$$(6) \quad f_\Gamma(y) \propto \lambda_\Gamma(y) = \frac{1}{\sqrt{-\det \text{CM}(2\pi\Gamma)}} \exp\left(-\frac{1}{2} (y \quad \mathbf{1}) \text{CM}(\Gamma)^{-1} \begin{pmatrix} y \\ \mathbf{1} \end{pmatrix}\right).$$

Here, $\text{CM}(\Gamma) := \begin{pmatrix} -\Gamma/2 & \mathbf{1} \\ \mathbf{1}^\top & 0 \end{pmatrix}$ is the Cayley–Menger matrix (Devriendt, 2022; Devriendt et al., 2026). Let $P := I - \frac{1}{d}\mathbf{1}\mathbf{1}^\top$ be a projection matrix onto $\mathbf{1}^\perp$, and define

$$(7) \quad \Sigma := -\frac{1}{2} P \Gamma P.$$

The variogram is recovered from Σ via $\Gamma = \text{diag}(\Sigma)\mathbf{1}^\top + \mathbf{1}\text{diag}(\Sigma)^\top - 2\Sigma$. If $\Gamma \in \mathcal{D}^d$, then Σ is positive semidefinite with kernel $\text{span}(\mathbf{1})$ and has a Moore–Penrose pseudoinverse $\Theta = \Sigma^+$. We write Γ_Θ for the variogram associated with a precision Θ via this identity (with $\Sigma = \Theta^+$). The matrix Θ allows for a parametric encoding of HRGMs: $\Theta_{ij} = 0$ is equivalent to the extremal conditional independence of Y_i and Y_j given the remaining coordinates (Hentschel et al., 2025). Furthermore, for Hüsler–Reiss distributions, the restriction for Θ to be a graph Laplacian matrix ($\Theta_{ij} \leq 0$ for all $i \neq j$) is equivalent to an extremal notion of total positivity (EMTP₂), compare Röttger et al. (2023).

Assuming i.i.d. data for some random vector X in the domain of attraction of a Hüsler–Reiss random vector Y as in (5), the empirical variogram estimator $\bar{\Gamma}$ of Engelke and Volgushev (2022) is a consistent estimator of Γ , which can serve as a summary statistic for parameter estimation in HRGMs (Hentschel et al., 2025). In order to estimate Θ for HRGMs under the constraint of EMTP₂, Röttger et al. (2023) propose a surrogate MLE under graph Laplacian constraint via the LCGGM log-likelihood with sample covariance $\bar{\Sigma} = -\frac{1}{2} P \bar{\Gamma} P$, that is

$$(8) \quad \hat{\Theta} = \arg \max_{\Theta} \ell(\Theta; \bar{\Sigma}) \quad \text{s.t. } \Theta_{ij} \leq 0, \quad \forall i \neq j.$$

Note that we can use this relationship between both estimation procedures to apply results and algorithms from LCGGM to Hüsler–Reiss.

3. LAPLACIAN-CONSTRAINED GAUSSIAN GRAPHICAL MODELS

3.1. Theory. The LCGGM-MLE \hat{K} obtained from a sample covariance S via (4) is by construction a connected graph Laplacian, so Theorem 2.1 applies directly: there exists a sparsifier \tilde{K} that is also a connected graph Laplacian and satisfies the spectral approximation

$$(9) \quad (1 - \varepsilon)\hat{K} \preceq \tilde{K} \preceq (1 + \varepsilon)\hat{K} \quad \text{on } \mathbf{1}^\perp.$$

We use the notation

$$(10) \quad D_{\text{KL}}^\perp(\hat{K} \parallel \tilde{K}) := \frac{1}{2} [\text{tr}(\tilde{K} \hat{K}^+) - (d - 1) - \log \text{Det}(\tilde{K} \hat{K}^+)]$$

for the KL divergence between the two centered degenerate Gaussians on $\mathbf{1}^\perp$ with precisions \hat{K} and \tilde{K} . See Lemma A.3 for the derivation.

Our goal is to control the LCGGM log-likelihood gap $\ell(\tilde{K}; T) - \ell(\hat{K}; T)$ induced by replacing \hat{K} by its sparsifier \tilde{K} , for any (projected) sample covariance matrix T supported on $\mathbf{1}^\perp$ (i.e., $T\mathbf{1} = 0$). The theorem below decomposes this gap into a structural cost (the KL term, which is the optimization-side price of moving away from \hat{K}) and a data residual (a trace term that vanishes when $T = \hat{K}^+$), and bounds it linearly in ε in both directions. Two regimes are worth distinguishing. If $T = S$

(in-sample evaluation), then \widehat{K} is the constrained MLE on S over the cone of connected Laplacians, so by definition no feasible \widetilde{K} can improve the in-sample log-likelihood and the gap is non-positive. If instead $T \neq S$, for instance when T is the sample covariance of held-out test data, the data residual $\text{tr}((\widetilde{K} - \widehat{K})(T - \widehat{K}^+))$ can take either sign, and the sparsifier may improve the log-likelihood on T relative to \widehat{K} .

Theorem 3.1. *Let $\varepsilon \in (0, 1)$, let $\widehat{K}, \widetilde{K}$ be connected graph Laplacians satisfying (9), and let $T \succeq 0$ be symmetric with $T\mathbf{1} = 0$. Then*

$$(11) \quad \ell(\widetilde{K}; T) - \ell(\widehat{K}; T) = -2D_{\text{KL}}^\perp(\widehat{K} \parallel \widetilde{K}) - \text{tr}((\widetilde{K} - \widehat{K})(T - \widehat{K}^+)),$$

and, setting $R(T) := \|\widehat{K}^{1/2}(T - \widehat{K}^+)\widehat{K}^{1/2}\|_*$ (with $\widehat{K}^{1/2}$ the symmetric square root of \widehat{K} on $\mathbf{1}^\perp$, zero on $\text{span}(\mathbf{1})$, and $\|\cdot\|_*$ the trace norm),

$$(12) \quad \ell(\widetilde{K}; T) - \ell(\widehat{K}; T) \leq \varepsilon R(T),$$

$$(13) \quad -\frac{(d-1)\varepsilon^2}{2(1-\varepsilon)} - \varepsilon R(T) \leq \ell(\widetilde{K}; T) - \ell(\widehat{K}; T) \leq \varepsilon R(T).$$

Beyond the log-likelihood bound, any sparsifier \widetilde{K} satisfying (9) is automatically a valid LCGGM precision matrix, with algebraic connectivity (the smallest nonzero eigenvalue λ_2 , also called the Fiedler eigenvalue) preserved within $1 \pm \varepsilon$.

Theorem 3.1 guarantees that any spectral sparsifier of \widehat{K} loses only an $O(\varepsilon)$ amount of in-sample log-likelihood. This motivates the three-step pipeline of Algorithm 1: (1) compute the dense LCGGM-MLE \widehat{K} (4) on the sample covariance S , (2) apply the BSS sparsifier of Theorem 2.1 to \widehat{K} , and (3) refit the LCGGM-MLE restricted to the edges retained by BSS.

The same algorithm applies to the Hüsler–Reiss setting of Section 4: the LCGGM-MLE (4) and the EMTP₂ surrogate HR-MLE (8) solve the same convex program $\arg \max\{\ell(K; D) : K \in \mathcal{C}\}$ over the cone \mathcal{C} of connected graph Laplacians, with only the input D changing (S for LCGGM, the data summary $\overline{\Sigma}$ for HR). Algorithm 1 is stated with D as input.

Algorithm 1: Spectral-LCGGM and Spectral-HR (unified).

Input: Data summary $D \in \mathbb{R}^{d \times d}$ (S for LCGGM, $\overline{\Sigma}$ for HR); BSS parameter $\eta > 1$.

Output: Sparse precision Laplacian $\widetilde{L}^{\text{refit}}$.

Step 1: Dense MLE: $L \leftarrow \arg \max\{\ell(K; D) : K \in \mathcal{C}\}$, with \mathcal{C} the cone of connected graph Laplacians

Step 2: BSS sparsification: run Theorem 2.1 on L at η , obtaining \widetilde{L} on $\leq \lceil \eta(d-1) \rceil$ edges satisfying $(1-\varepsilon)L \preceq \widetilde{L} \preceq (1+\varepsilon)L$ on $\mathbf{1}^\perp$, with $\varepsilon = (\kappa(\eta) - 1)/(\kappa(\eta) + 1)$; set

$$\widetilde{E} \leftarrow \{(i, j) : \widetilde{L}_{ij} \neq 0, i \neq j\}$$

Step 3: Refit: return $\widetilde{L}^{\text{refit}} \leftarrow \arg \max\{\ell(K; D) : K \in \mathcal{C}, \text{supp}(K) \subseteq \widetilde{E}\}$

Tuning proceeds through η , selected by BIC on the training data; smaller η yields sparser subgraphs at looser spectral certificates.

3.2. Experiments. We evaluate Spectral-LCGGM on simulated data drawn from an LCGGM whose ground-truth precision K^* is the Laplacian of a weighted random graph (the specific graph families and dimensions are detailed below), so E^* denotes the edge set of that random graph. For each method, we report the edge count $|\widehat{E}|$ (number of off-diagonals of the estimate exceeding 10^{-3} in

magnitude), the precision $|\widehat{E} \cap E^*|/|\widehat{E}|$, the recall $|\widehat{E} \cap E^*|/|E^*|$, and the F1 score (harmonic mean of precision and recall), together with the LCGGM test log-likelihood $\ell(\widehat{K}; S_{\text{test}})$ on a held-out sample covariance. Tuning parameters are selected on the training split by the Bayesian information criterion (BIC)

$$(14) \quad \text{BIC}(M) := -n_{\text{train}} \ell(M; D_{\text{train}}) + k(M) \log n_{\text{train}},$$

with ℓ the LCGGM log-likelihood (3), n_{train} the number of training data points, D_{train} the training covariance in each setting, and $k(M)$ the edge count of the graph given by the Laplacian M .

We compare Spectral-LCGGM (Algorithm 1) against two baselines that span the sparsity–fit trade-off: CGL (Egilmez et al., 2017), the unpenalized LCGGM-MLE and NGL-SCAD (Ying et al., 2020), a nonconvex SCAD-penalized LCGGM solver. The Graphical Lasso is excluded because ℓ_1 -norm penalization is known not to produce sparse estimates in the LCGGM setting (Ying et al., 2020).

The ground-truth precision matrix K^* is the Laplacian of a weighted random graph, with edge weights drawn from $\text{Unif}[0.5, 1.5]$ to avoid eigenvalue multiplicities. We consider two random graph families: Erdős–Rényi (ER) graphs with uniform degree, and stochastic block models (SBM) with five blocks ($p_{\text{in}} = 0.12$, $p_{\text{out}} = 0.01$) inducing community structure. Each topology is realized at two dimensions, $d \in \{100, 200\}$, with $n_{\text{train}} = 4d$ training and $n_{\text{test}} = 4,000$ test observations, over $B = 10$ replications.

Table 1 reports the BIC-selected results. Across all four settings the unpenalized LCGGM-MLE (CGL) recovers a graph much denser than the truth, with high recall and very low precision. NGL-SCAD (BIC-selected α) brings the edge count closer to the truth with substantially improved F1. Spectral-LCGGM consistently delivers edge counts within 5% of the truth and achieves the highest F1 (≥ 0.94) in every setting, while also obtaining the best test log-likelihood. The test log-likelihood gap to NGL-SCAD is narrow, reflecting that NGL-SCAD also fits the data well; Spectral-LCGGM’s advantage materialises primarily on graph recovery.

Setting	Method	Edges	Precision	Recall	F1	Test log-lik.
ER, $d = 100$ $ E^* = 176$	CGL	506.3 (4.9)	0.348 (0.003)	1.000 (0.000)	0.516 (0.004)	−8,173 (125)
	NGL-SCAD	240.7 (2.8)	0.731 (0.008)	0.999 (0.001)	0.844 (0.005)	−7,269 (123)
	Spectral-LCGGM	185.0 (1.0)	0.950 (0.006)	0.998 (0.001)	0.973 (0.003)	−6,631 (135)
SBM, $d = 100$ $ E^* = 171$	CGL	453.9 (4.9)	0.377 (0.004)	1.000 (0.000)	0.548 (0.004)	−27,284 (141)
	NGL-SCAD	233.7 (2.0)	0.731 (0.007)	0.998 (0.001)	0.844 (0.005)	−26,378 (146)
	Spectral-LCGGM	176.6 (0.7)	0.963 (0.004)	0.995 (0.001)	0.979 (0.002)	−25,952 (141)
ER, $d = 200$ $ E^* = 391$	CGL	1,259.5 (8.4)	0.311 (0.002)	1.000 (0.000)	0.474 (0.002)	19,469 (253)
	NGL-SCAD	488.6 (9.1)	0.801 (0.014)	0.998 (0.000)	0.888 (0.009)	21,085 (269)
	Spectral-LCGGM	392.9 (0.5)	0.992 (0.001)	0.997 (0.001)	0.994 (0.001)	21,889 (229)
SBM, $d = 200$ $ E^* = 623$	CGL	1,886.9 (16.8)	0.329 (0.003)	0.995 (0.001)	0.494 (0.003)	248,258 (242)
	NGL-SCAD	781.4 (1.8)	0.770 (0.002)	0.966 (0.002)	0.857 (0.002)	249,607 (234)
	Spectral-LCGGM	632.8 (1.9)	0.936 (0.003)	0.950 (0.002)	0.943 (0.002)	250,223 (246)

TABLE 1. LCGGM simulation across two topologies and two dimensions ($d \in \{100, 200\}$). The two topologies are Erdős–Rényi (ER) with target density $2(d-1)$ edges, and stochastic block model (SBM) with five equal-sized blocks, $p_{\text{in}} = 0.12$, $p_{\text{out}} = 0.01$ (so the true edge count $|E^*|$ grows with d). Means over $B = 10$ replications with standard errors in parentheses. Bold: best on each metric within each (d , topology) block.

4. HÜSLER-REISS GRAPHICAL MODELS

4.1. Theory. Under EMTP₂, the precision matrix Θ is a graph Laplacian (Section 2.3), so Theorem 2.1 applies directly to Θ . Moreover, by (8) the surrogate Hüsler-Reiss MLE $\hat{\Theta}$ is the LCGGM-MLE (4) evaluated at $\bar{\Sigma}$ in place of the sample covariance. No separate analysis is therefore required for the Hüsler-Reiss case: the LCGGM theory of Section 3.1 transfers verbatim under the substitution $\hat{K} \rightarrow \hat{\Theta}$, $\tilde{K} \rightarrow \tilde{\Theta}$, $S \rightarrow \bar{\Sigma}$, $\hat{K}^+ \rightarrow \hat{\Sigma} = \hat{\Theta}^+$, with the spectral approximation

$$(15) \quad (1 - \varepsilon)\hat{\Theta} \preceq \tilde{\Theta} \preceq (1 + \varepsilon)\hat{\Theta} \quad \text{on } \mathbf{1}^\perp$$

in place of (9). The unified estimator of Algorithm 1, run with $\hat{\Theta}$ and $D = \bar{\Sigma}$, produces Spectral-HR. Concretely, Theorem 3.1 gives

$$(16) \quad \ell(\tilde{\Theta}; T) - \ell(\hat{\Theta}; T) = -2D_{\text{KL}}^\perp(\hat{\Theta} \parallel \tilde{\Theta}) - \text{tr}((\tilde{\Theta} - \hat{\Theta})(T - \hat{\Sigma}))$$

and, with $\gamma(T) = \text{diag}(T)\mathbf{1}^\top + \mathbf{1}\text{diag}(T)^\top - 2T$ we have for $R_{\hat{\Gamma}} := \|\hat{\Theta}^{1/2}(T - \hat{\Sigma})\hat{\Theta}^{1/2}\|_* = \frac{1}{2}\|\hat{\Theta}^{1/2}P(\gamma(T) - \hat{\Gamma})P\hat{\Theta}^{1/2}\|_*$ (the subscript reflects the underlying variogram-estimation error), that

$$(17) \quad -\frac{(d-1)\varepsilon^2}{2(1-\varepsilon)} - \varepsilon R_{\hat{\Gamma}} \leq \ell(\tilde{\Theta}; \bar{\Sigma}) - \ell(\hat{\Theta}; \bar{\Sigma}) \leq \varepsilon R_{\hat{\Gamma}}.$$

Under any consistent variogram estimator, $R_{\hat{\Gamma}} \rightarrow 0$ in probability, so the residual term in (17) vanishes asymptotically. Any sparsifier $\tilde{\Theta}$ satisfying (15) is itself a connected graph Laplacian (by construction of BSS), hence the precision of an EMTP₂ Hüsler-Reiss distribution, with algebraic connectivity λ_2 preserved within $1 \pm \varepsilon$.

The remainder of this subsection collects two guarantees with relevance to the Hüsler-Reiss case: all variogram entries Γ_{ij} are preserved multiplicatively, and the Hüsler-Reiss logarithmic exponent measure density $\log \lambda(y)$ is controlled pointwise.

Theorem 4.1. *Let $\Theta, \tilde{\Theta}$ be connected graph Laplacians satisfying (15), with associated variograms $\Gamma, \tilde{\Gamma}$. For every pair $i \neq j$,*

$$(18) \quad \frac{\Gamma_{ij}}{1 + \varepsilon} \leq \tilde{\Gamma}_{ij} \leq \frac{\Gamma_{ij}}{1 - \varepsilon}.$$

In other words, the variogram is preserved multiplicatively within a factor $1/(1 \pm \varepsilon)$, independently of d and $\lambda_2(\Theta)$.

The multiplicative variogram control transfers, via the Cayley-Menger representation (6), to a pointwise bound on the Hüsler-Reiss logarithmic exponent measure density. Before stating it, define

$$(19) \quad M_\Theta := \|\text{CM}(\Gamma)^{-1}\|_{\text{op}} \leq \|\Theta\|_{\text{op}} + \|p\|_2 + |\sigma^2|,$$

where $\Theta \in \mathbb{R}^{d \times d}$, $p \in \mathbb{R}^d$, and $\sigma^2 \in \mathbb{R}$ are the blocks of $\text{CM}(\Gamma)^{-1} = \begin{pmatrix} \Theta & p \\ p^\top & \sigma^2 \end{pmatrix}$, with $\Theta = \Sigma^+$ in the top-left $d \times d$ block (Fiedler-Bapat identity, see Devriendt (2022)). Set also $\eta_C := \varepsilon \|\Gamma\|_2 / (2(1 - \varepsilon))$.

Corollary 4.2. *Let $\Theta, \tilde{\Theta}$ be connected graph Laplacians satisfying (15), with associated variograms $\Gamma, \tilde{\Gamma}$, and suppose $\eta_C M_\Theta < 1$. Then for every $y \in \mathcal{E}$,*

$$(20) \quad |\log \lambda_{\tilde{\Gamma}}(y) - \log \lambda_\Gamma(y)| \leq \frac{d+1}{2} \cdot \frac{\eta_C M_\Theta}{1 - \eta_C M_\Theta} + \frac{\|y\|_2^2 + 1}{2} \cdot \frac{\eta_C M_\Theta^2}{1 - \eta_C M_\Theta},$$

and for any sample $Y_1, \dots, Y_n \in \mathcal{E}$ with $\|Y\|^2 := n^{-1} \sum_k \|Y_k\|_2^2$,

$$(21) \quad \frac{1}{n} \left| \sum_{k=1}^n [\log \lambda_{\tilde{\Gamma}}(Y_k) - \log \lambda_\Gamma(Y_k)] \right| \leq \frac{d+1}{2} \cdot \frac{\eta_C M_\Theta}{1 - \eta_C M_\Theta} + \frac{\|Y\|^2 + 1}{2} \cdot \frac{\eta_C M_\Theta^2}{1 - \eta_C M_\Theta}.$$

Both bounds are $O(\varepsilon)$ as $\varepsilon \downarrow 0$ and independent of the spectral gap $\lambda_2(\Theta)$. The sample-average bound (21) controls the data-dependent part of the Hüsler–Reiss log-likelihood: writing $\ell^{\text{HR}}(\Theta; Y_{1:n}) = \sum_k \log \lambda_\Gamma(Y_k) - n \log V(\Gamma)$, the remaining term $\log V(\tilde{\Gamma}) - \log V(\Gamma)$ is deterministic in $\Gamma, \tilde{\Gamma}$ and depends only on the variogram perturbation $\tilde{\Gamma} - \Gamma$, which is itself controlled multiplicatively by (18). We do not develop an explicit bound on this term here. The condition $\eta_C M_\Theta < 1$ holds for any fixed Θ once ε is small enough.

4.2. Experiments. We evaluate Spectral-HR against the EMTP₂-MLE (Röttger et al., 2023) and the two majority-vote variants of eglearn (Engelke et al., 2025), neighborhood-selection (eglearn-NS) and graphical-lasso (eglearn-glasso), on two Hüsler–Reiss real-data benchmark datasets. The upper Danube river-network discharge dataset (Engelke and Hitz, 2020) has a modest sample size, which makes it difficult to split the data with a high enough sample size (having in mind that we also have to threshold the data), so methods are compared by BIC and AIC on the full thresholded sample. The Texas Cluster of U.S. airports (Hentschel et al., 2025) is a much larger dataset, so we can use the standard train/test date split of Hentschel et al. (2025) and held-out Hüsler–Reiss log-likelihood as the headline metric. In both experiments the log-likelihood used for selection and held-out evaluation is the actual Hüsler–Reiss log-likelihood $\ell^{\text{HR}}(\hat{\Theta}) := \sum_k \log f_{\hat{\Gamma}}(Y_k)$.

Upper Danube river-network discharges (Engelke and Hitz, 2020). This is a standard Hüsler–Reiss benchmark. The data are daily seasonal-residual discharges at $d = 31$ gauging stations along the upper Danube and its tributaries, with $n = 428$ exceedance-cluster days as bundled in the `graphicalExtremes` R package. Since there is no canonical extremal ground-truth graph for river discharges, we use the whole dataset both for fitting and for the tuning criteria, and compare methods purely on in-sample model selection. At threshold $p = 0.90$ the thresholded sample has $n^{\text{thr}} = 117$ exceedances, on which we evaluate both

$$(22) \quad \text{BIC}(\hat{\Theta}) = -2 \ell^{\text{HR}}(\hat{\Theta}) + k(\hat{\Theta}) \log n^{\text{thr}}, \quad \text{AIC}(\hat{\Theta}) = -2 \ell^{\text{HR}}(\hat{\Theta}) + 2k(\hat{\Theta}),$$

where $k(\hat{\Theta})$ is the edge count of the graph given by $\hat{\Theta}$. Each tunable method is selected twice: once by BIC, once by AIC. The EMTP₂-MLE has no tuning parameter. Tuning grids are $\rho \in [0.005, 0.5]$ for eglearn-NS, $\rho \in [0.005, 0.75]$ (20 equidistant points) for eglearn-glasso, and $\eta \in [1.1, 100]$ for Spectral-HR.

Table 2 reports the BIC- and AIC-selected fits. Spectral-HR gives the sparsest fits by a clear margin (46–53 edges, vs 99–130 for eglearn-NS, 171 for eglearn-glasso, and 67 for EMTP₂). eglearn-NS attains both the best BIC and the best AIC, at much higher edge counts than Spectral-HR. Against the dense EMTP₂ baseline, Spectral-HR improves both criteria ($\Delta\text{BIC} = -71.6$, $\Delta\text{AIC} = -28.6$) while using roughly 70% of its edges; it trails the eglearn-NS winners on the absolute criteria (87 BIC points / 302 AIC points behind), trading information-criterion fit for substantially sparser graphs.

Spectral-HR’s edge count grows monotonically over η and stays below EMTP₂’s 67 edges across the entire grid. eglearn-NS admits a usable fit only for $\rho < 0.132$, and past the BIC-selected $\rho = 0.032$ both criteria rise above the dense EMTP₂ baseline; eglearn-glasso attains its joint BIC/AIC minimum at the second grid point ($\rho = 0.044$, 171 edges). Full sweeps are in Table 4 (Section B), where we observe that the eglearn performance decays for stronger sparsity settings. Therefore, our impression for the Danube data set is that our method behaves better if we are looking for a sparser model with reasonable performance.

Texas Cluster of U.S. airports (Hentschel et al., 2025). The data are daily total flight delays at $d = 29$ airports, accessed via the `graphicalExtremes` R package, with the predefined train/test date split of Hentschel et al. (2025) ($n_{\text{train}} = 1,764$, $n_{\text{test}} = 1,839$ days). At threshold $p = 0.85$ this yields $n_{\text{tr}}^{\text{thr}} = 1,069$ training and $n_{\text{te}}^{\text{thr}} = 1,336$ held-out exceedances. There is no canonical extremal

Method	Selected by	Param	Edges	BIC	AIC
EMTP ₂	(none)	–	67	1,336.07	1,150.98
eglearn-NS	BIC	0.032	99	1,177.01	903.54
	AIC	0.023	130	1,179.36	820.30
eglearn-glasso	BIC & AIC	0.044	171	1,342.77	870.42
Spectral-HR	BIC	4	46	1,264.46	1,137.40
	AIC	25	53	1,268.75	1,122.34

TABLE 2. Upper Danube river-network discharges (Hüsler-Reiss, $d = 31$, $n = 428$ days, threshold $p = 0.90$, $n^{\text{thr}} = 117$ exceedances). Whole dataset used for fitting and for both selection criteria (22). Each tunable method appears twice, once with its BIC-selected parameter and once with its AIC-selected parameter. Bold: lowest BIC and lowest AIC across all rows.

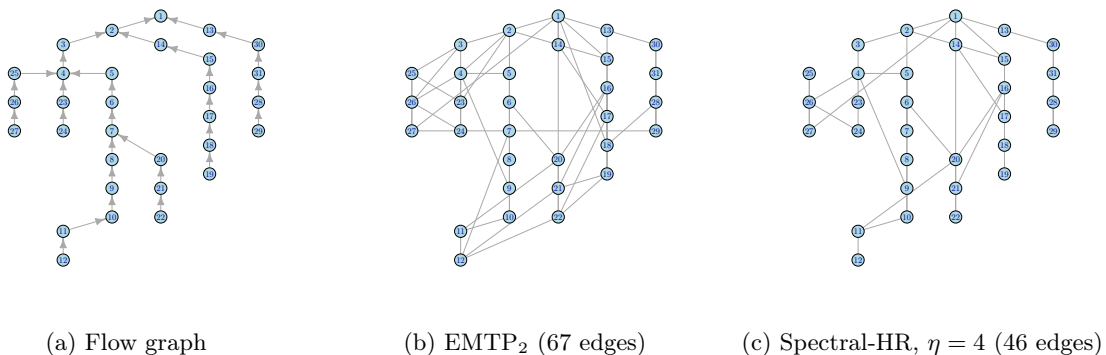


FIGURE 1. Danube river network: (a) the directed flow graph from Engelke and Hitz (2020); (b) the EMTP₂-MLE fit; and (c) the Spectral-HR fit at the BIC-selected $\eta = 4$. Node positions and numbering match across panels.

ground-truth graph for flight delays, so we evaluate each fit by edge count, training Hüsler-Reiss BIC (the tuning criterion), and held-out Hüsler-Reiss log-likelihood. Tuning grids ($\rho \in [0.005, 0.5]$ for eglearn, $\eta \in [1.1, 100]$ for Spectral-HR) are chosen wide enough that the BIC-selected parameter is interior on the grid.

Table 3 reports the BIC-selected results. Spectral-HR gives the sparsest fit by a clear margin (95 edges, vs 130 for EMTP₂ and 211–227 for the eglearn variants). EMTP₂ attains the best held-out test log-likelihood, with Spectral-HR a close second ($-23,104$ vs $-23,209$) at a 27% reduction in edge count. The eglearn variants achieve the best training BIC but visibly overfit: their held-out log-likelihoods ($-23,851$ and $-23,900$) are substantially worse than both EMTP₂ and Spectral-HR despite the lower training BIC.

5. DISCUSSION

We extended the post-estimation spectral-sparsification approach of Echave-Sustaeta Rodríguez et al. (2026) from the full-rank Gaussian MTP₂ setting to two families of graphical models with a

Method	Edges	Train BIC	HR test log-lik.
EMTP ₂	130	38,135.6	−23,104.1
eglearn-NS	211	37,288.9	−23,899.8
eglearn-glasso	227	37,369.6	−23,851.3
Spectral-HR	95	37,967.5	−23,208.8

TABLE 3. Texas Cluster of U.S. airports, daily total flight delays (Hüsler–Reiss, $d = 29$, training/test split sizes $n_{\text{train}} = 1,764$, $n_{\text{test}} = 1,839$ from Hentschel et al. (2025), threshold $p = 0.85$; training/test exceedance counts $n_{\text{tr}}^{\text{thr}} = 1,069$, $n_{\text{te}}^{\text{thr}} = 1,336$). Tuning by Hüsler–Reiss BIC on the training sample; selected parameters $\rho = 0.032$ (eglearn-NS), $\rho = 0.05$ (eglearn-glasso), $\eta = 20$ (Spectral-HR). Train BIC is the tuning criterion $-2\ell^{\text{HR}}(\hat{\Theta}; Y_{\text{thr}}^{\text{tr}}) + k(\hat{\Theta}) \log n_{\text{tr}}^{\text{thr}}$; the last column is the held-out Hüsler–Reiss log-likelihood. Bold: best on each metric.

graph Laplacian precision matrix, the LCGGM and the EMTP₂ HRGM. Given that both models are estimated in a similar way, we can use the same algorithm in both settings. In each setting we run BSS on the dense estimator and refit on the sparsified support. A Bregman–Loewner identity on $\mathbf{1}^\perp$ underpins the analysis of both settings.

The powerful spectral sparsification tools, together with the models we consider, ensure that the sparsified matrices are still valid statistical parameters that are spectrally close to the original ones. For HRGMs, we provide additional guarantees. We evaluate Spectral-LCGGM empirically in simulations, where we observe that our method serves as a post-processing operation which reduces the complexity of the model while keeping performance high, or even improving it in some instances. We also observe that our proposed method seems to be quite precise at structure learning in this setting.

Additionally, we evaluate Spectral-HR in two real data examples, where we observe that in practice our method seems to offer a trade-off between model fit and complexity: we do not necessarily improve the model fit, but we manage to simplify it without significant loss in performance.

Regarding future work, we believe there is still much to explore around these methods. First, we believe that the refit step could be modified to include constraints beyond positivity. Currently, we refit by imposing the sparsified support under a Laplacian constraint, but we would like to explore whether other refitting options behave differently. Additionally, one may consider other spectral sparsification methods for the sparsification step. Regarding the performance of our methods, we believe it is possible to obtain more detailed theory specific to Spectral-HR, and overall we would find it interesting to see whether support recovery results are achievable, since the methods seem to recover structure quite well in simulations. Finally, we would like to explore more settings for simulations and real data experiments to further support our methods with additional empirical evidence of their performance.

ACKNOWLEDGEMENTS

The research of Aida Abiad is supported by NWO (Dutch Research Council) through the grant VI.Vidi.213.085.

REFERENCES

Joshua Batson, Daniel A. Spielman, and Nikhil Srivastava. Twice-Ramanujan sparsifiers. *SIAM Journal on Computing*, 41(6):1704–1721, 2012. doi: 10.1137/090772873.

- Jian-Feng Cai, José Vinícius de Miranda Cardoso, Daniel P. Palomar, and Jiayi Ying. Fast projected newton-like method for precision matrix estimation under total positivity. In *Advances in Neural Information Processing Systems*, volume 36, pages 73348–73370. Curran Associates, Inc., 2023. URL https://proceedings.neurips.cc/paper_files/paper/2023/file/e878c8f38381d0964677fb9536c494ee-Paper-Conference.pdf.
- Daniele Calandriello, Alessandro Lazaric, Ioannis Koutis, and Michal Valko. Improved large-scale graph learning through ridge spectral sparsification. In *Proceedings of the 35th International Conference on Machine Learning*, volume 80 of *Proceedings of Machine Learning Research*, pages 688–697. PMLR, 2018. URL <https://proceedings.mlr.press/v80/calandriello18a.html>.
- Karel Devriendt. *Graph geometry from effective resistances*. PhD thesis, University of Oxford, 2022.
- Karel Devriendt, Ignacio Echave-Sustaeta Rodríguez, and Frank Röttger. Extremal conditional independence for hüsler–reiss distributions via modular functions. *arXiv preprint arXiv:2601.21931*, 2026.
- Ignacio Echave-Sustaeta Rodríguez, Aida Abiad, and Frank Röttger. Learning Gaussian graphical models under total positivity via spectral graph sparsification, 2026. URL <https://arxiv.org/abs/2605.17154>.
- Hilmi E. Egilmez, Eduardo Pavez, and Antonio Ortega. Graph learning from data under Laplacian and structural constraints. *IEEE Journal of Selected Topics in Signal Processing*, 11(6):825–841, 2017. doi: 10.1109/JSTSP.2017.2726975.
- Sebastian Engelke and Adrien S. Hitz. Graphical models for extremes. *Journal of the Royal Statistical Society Series B: Statistical Methodology*, 82(4):871–932, 2020. ISSN 1369-7412. doi: 10.1111/rssb.12355.
- Sebastian Engelke and Stanislav Volgushev. Structure learning for extremal tree models. *Journal of the Royal Statistical Society Series B: Statistical Methodology*, 84(5):2055–2087, 11 2022. ISSN 1369-7412. doi: 10.1111/rssb.12556. URL <https://doi.org/10.1111/rssb.12556>.
- Sebastian Engelke, Michaël Lalancette, and Stanislav Volgushev. Learning extremal graphical structures in high dimensions, 2025. URL <https://arxiv.org/abs/2111.00840>. To appear in the *Annals of Statistics*.
- Manuel Hentschel, Sebastian Engelke, and Johan Segers. Statistical inference for Hüsler–Reiss graphical models through matrix completions. *Journal of the American Statistical Association*, 120(550):909–921, 2025. doi: 10.1080/01621459.2024.2371978.
- Ioannis Koutis, Alex Levin, and Richard Peng. Improved spectral sparsification and numerical algorithms for SDD matrices. In *Proceedings of the 29th International Symposium on Theoretical Aspects of Computer Science (STACS’12)*, pages 266–277, 2012. doi: 10.4230/LIPIcs.STACS.2012.266.
- Sandeep Kumar, Jiayi Ying, José Vinícius de Miranda Cardoso, and Daniel P. Palomar. A unified framework for structured graph learning via spectral constraints. *Journal of Machine Learning Research*, 21(22):1–60, 2020. URL <http://jmlr.org/papers/v21/19-276.html>.
- Rasmus Kyng and Sushant Sachdeva. Approximate Gaussian elimination for Laplacians: Fast, sparse, and simple. In *2016 IEEE 57th Annual Symposium on Foundations of Computer Science (FOCS)*, pages 573–582. IEEE, 2016. doi: 10.1109/FOCS.2016.68.
- Steffen L. Lauritzen. *Graphical Models*. Oxford University Press, 1996. ISBN 978-0-19-852219-5.
- Steffen L. Lauritzen, Caroline Uhler, and Piotr Zwiernik. Maximum likelihood estimation in Gaussian models under total positivity. *The Annals of Statistics*, 47(4):1835–1863, 2019. doi: 10.1214/17-AOS1668.
- H. Rootzén and N. Tajvidi. Multivariate generalized Pareto distributions. *Bernoulli*, 12(5):917–930, 2006. doi: 10.3150/bj/1161614952.
- Frank Röttger, Sebastian Engelke, and Piotr Zwiernik. Total positivity in multivariate extremes. *The Annals of Statistics*, 51(3):962–1004, 2023. ISSN 0090-5364,2168-8966. doi: 10.1214/23-AOS2272.

URL <https://doi.org/10.1214/23-AOS2272>.

Veeru Sadhanala, Yu-Xiang Wang, and Ryan J. Tibshirani. Graph sparsification approaches for Laplacian smoothing. In *Proceedings of the 19th International Conference on Artificial Intelligence and Statistics*, volume 51 of *Proceedings of Machine Learning Research*, pages 1250–1259. PMLR, 2016. URL <https://proceedings.mlr.press/v51/sadhanala16.html>.

Martin Slawski and Matthias Hein. Estimation of positive definite M-matrices and structure learning for attractive Gaussian Markov random fields. *Linear Algebra and its Applications*, 473:145–179, 2015.

Daniel A. Spielman and Nikhil Srivastava. Graph sparsification by effective resistances. *SIAM Journal on Computing*, 40(6):1913–1926, 2011. doi: 10.1137/080734029.

Daniel A. Spielman and Shang-Hua Teng. Nearly-linear time algorithms for graph partitioning, graph sparsification, and solving linear systems. In *Proceedings of the 36th Annual ACM Symposium on Theory of Computing (STOC’04)*, pages 81–90, 2004. doi: 10.1145/1007352.1007372.

Nikhil Srivastava and Roman Vershynin. Covariance estimation for distributions with $2+\epsilon$ moments. *Annals of Probability*, 41(5):3081–3111, 2013. doi: 10.1214/12-AOP760.

Yongyu Wang, Zhiqiang Zhao, and Zhuo Feng. Scalable graph topology learning via spectral densification. In *Proceedings of the 15th ACM International Conference on Web Search and Data Mining*, pages 1099–1108. ACM, 2022. doi: 10.1145/3488560.3498480. URL <https://dl.acm.org/doi/10.1145/3488560.3498480>.

Yuhao Wang, Uma Roy, and Caroline Uhler. Learning high-dimensional Gaussian graphical models under total positivity without adjustment of tuning parameters. In *Proceedings of the Twenty Third International Conference on Artificial Intelligence and Statistics (AISTATS 2020)*, volume 108 of *Proceedings of Machine Learning Research*, pages 2698–2708. PMLR, 2020. URL <https://proceedings.mlr.press/v108/wang20g.html>.

Jiaxi Ying, José Vinícius de Miranda Cardoso, and Daniel P. Palomar. Nonconvex sparse graph learning under Laplacian constrained graphical model. In *Advances in Neural Information Processing Systems*, volume 33, pages 7101–7113. Curran Associates, Inc., 2020. URL https://proceedings.neurips.cc/paper_files/paper/2020/file/4ef42b32bcc9485b10b8183507e5d82-Paper.pdf.

APPENDIX A. PROOFS

A.1. Bregman–Loewner Lemmas. The proof of Theorem 3.1 (which, applied under the substitution of Section 4.1, also yields the Hüsler–Reiss identities (16)–(17)) and the associated refit corollaries reduce to two elementary lemmas about graph Laplacians sharing the kernel $\text{span}(\mathbf{1})$. The full-rank versions of these lemmas, for positive definite matrices, were proved in Echave-Sustaeta Rodríguez et al. (2026, Sec. 3). The two statements below adapt them to the degenerate-rank setting that arises here for both LCGMs and the Hüsler–Reiss surrogate.

Lemma A.1. *Let K, \tilde{K} be positive semidefinite matrices with common kernel $\text{span}(\mathbf{1})$, and suppose $(1 - \epsilon)K \preceq \tilde{K} \preceq (1 + \epsilon)K$ on $\mathbf{1}^\perp$ for some $\epsilon \in (0, 1)$. Then $D_{\text{KL}}^\perp(K \| \tilde{K}) \geq 0$, and*

$$(23) \quad 2D_{\text{KL}}^\perp(K \| \tilde{K}) \leq \frac{(d-1)\epsilon^2}{2(1-\epsilon)}.$$

In particular, $2D_{\text{KL}}^\perp \leq (d-1)\epsilon^2$ for $\epsilon \leq \frac{1}{2}$.

Proof. Working on $\mathbf{1}^\perp$, let μ_1, \dots, μ_{d-1} be the eigenvalues of $\tilde{K}K^+$. The spectral approximation gives $\mu_i \in [1 - \epsilon, 1 + \epsilon]$. The standard KL identity for degenerate centered Gaussians on $\mathbf{1}^\perp$ is $2D_{\text{KL}}^\perp(K \| \tilde{K}) = \sum_{i=1}^{d-1} (\mu_i - 1 - \log \mu_i) \geq 0$. Writing $\mu_i = 1 + t_i$ with $|t_i| \leq \epsilon < 1$ and applying the bound $t - \log(1 + t) \leq t^2/(2(1 - |t|))$ for $|t| < 1$ (Taylor with integral remainder) yields $\mu_i -$

$1 - \log \mu_i \leq \varepsilon^2 / (2(1 - \varepsilon))$; summing gives (23). The simpler bound $(d - 1)\varepsilon^2$ follows for $\varepsilon \leq \frac{1}{2}$ since $1 / (2(1 - \varepsilon)) \leq 1$. \square

Lemma A.2. *Let K, \tilde{K} be positive semidefinite matrices with common kernel $\text{span}(\mathbf{1})$ and $-\varepsilon K \preceq \tilde{K} - K \preceq \varepsilon K$ on $\mathbf{1}^\perp$. Then for every symmetric matrix A supported on $\mathbf{1}^\perp$,*

$$|\text{tr}((\tilde{K} - K)A)| \leq \varepsilon \|K^{1/2}AK^{1/2}\|_*,$$

where $K^{1/2}$ is the symmetric square root of K on $\mathbf{1}^\perp$.

Proof. Let $V \in \mathbb{R}^{d \times (d-1)}$ have orthonormal columns spanning $\mathbf{1}^\perp$ and write $\bar{X} := V^\top XV$ for any symmetric matrix X supported on $\mathbf{1}^\perp$. Then $\text{tr}(XY) = \text{tr}(\bar{X}\bar{Y})$ for such matrices, and $\bar{K} \succ 0$. The spectral approximation is equivalent to $\|\bar{K}^{-1/2}(\tilde{K} - \bar{K})\bar{K}^{-1/2}\|_{\text{op}} \leq \varepsilon$. The operator-trace Hölder inequality gives

$$|\text{tr}((\tilde{K} - K)A)| = |\text{tr}(\bar{K}^{-1/2}(\tilde{K} - \bar{K})\bar{K}^{-1/2} \cdot \bar{K}^{1/2}\bar{A}\bar{K}^{1/2})| \leq \varepsilon \|\bar{K}^{1/2}\bar{A}\bar{K}^{1/2}\|_*,$$

and $\|\bar{K}^{1/2}\bar{A}\bar{K}^{1/2}\|_* = \|K^{1/2}AK^{1/2}\|_*$. \square

A.2. Proofs for Section 3.

Lemma A.3 (Closed form of the degenerate-Gaussian KL). *Let K, \tilde{K} be positive semidefinite matrices with common kernel $\text{span}(\mathbf{1})$. The KL divergence between the two centered degenerate Gaussians on $\mathbf{1}^\perp$ with precisions K and \tilde{K} is*

$$(24) \quad D_{\text{KL}}^\perp(K \parallel \tilde{K}) = \frac{1}{2} [\text{tr}(\tilde{K}K^+) - (d - 1) - \log \text{Det}(\tilde{K}K^+)] = \frac{1}{2} \sum_{i=1}^{d-1} (\mu_i - 1 - \log \mu_i),$$

where μ_1, \dots, μ_{d-1} are the eigenvalues of $\tilde{K}K^+$ on $\mathbf{1}^\perp$ (equivalently, the generalized eigenvalues of \tilde{K} relative to K on $\mathbf{1}^\perp$). In particular, $D_{\text{KL}}^\perp(K \parallel \tilde{K}) \geq 0$ with equality iff $\tilde{K} = K$ on $\mathbf{1}^\perp$.

Proof. On $\mathbf{1}^\perp$, both Gaussians are absolutely continuous with respect to the $(d - 1)$ -dimensional Lebesgue measure on that hyperplane, with densities

$$f_K(y) = \frac{(\text{Det}K)^{1/2}}{(2\pi)^{(d-1)/2}} \exp(-\frac{1}{2}y^\top Ky), \quad f_{\tilde{K}}(y) = \frac{(\text{Det}\tilde{K})^{1/2}}{(2\pi)^{(d-1)/2}} \exp(-\frac{1}{2}y^\top \tilde{K}y).$$

Both densities live on the same measure space because K and \tilde{K} share the kernel $\text{span}(\mathbf{1})$. The log-density difference equals $\frac{1}{2} \log \text{Det}K - \frac{1}{2} \log \text{Det}\tilde{K} - \frac{1}{2}y^\top (K - \tilde{K})y$. Taking expectation under $Y \sim f_K$ with $\mathbb{E}_K[YY^\top] = K^+$,

$$\mathbb{E}_K[Y^\top (K - \tilde{K})Y] = \text{tr}((K - \tilde{K})K^+) = \text{tr}(KK^+) - \text{tr}(\tilde{K}K^+) = (d - 1) - \text{tr}(\tilde{K}K^+),$$

using $KK^+ = P$, the projector onto $\mathbf{1}^\perp$ with $\text{tr}(P) = d - 1$. Substituting,

$$D_{\text{KL}}^\perp(K \parallel \tilde{K}) = \frac{1}{2} [\text{tr}(\tilde{K}K^+) - (d - 1) + \log \text{Det}K - \log \text{Det}\tilde{K}].$$

Since K and \tilde{K} share kernel $\text{span}(\mathbf{1})$, both are (pseudo-) invertible on $\mathbf{1}^\perp$ and the determinant product rule on $\mathbf{1}^\perp$ gives $\log \text{Det}K - \log \text{Det}\tilde{K} = -\log \text{Det}(\tilde{K}K^+)$, yielding the first equality in (24). For the second, let μ_i be the eigenvalues of $\tilde{K}K^+$ on $\mathbf{1}^\perp$; then $\text{tr}(\tilde{K}K^+) = \sum_i \mu_i$, $\log \text{Det}(\tilde{K}K^+) = \sum_i \log \mu_i$, and $d - 1 = \sum_i 1$, so the three terms combine into $\sum_i (\mu_i - 1 - \log \mu_i)$. Non-negativity, with equality iff every $\mu_i = 1$, follows from $\mu - 1 - \log \mu \geq 0$ for $\mu > 0$. \square

Proof of Theorem 3.1. By the KL identity for degenerate Gaussians on $\mathbf{1}^\perp$,

$$2D_{\text{KL}}^\perp(\widehat{K} \parallel \widetilde{K}) = \text{tr}(\widetilde{K}\widehat{K}^+) - (d-1) + \log \text{Det}\widehat{K} - \log \text{Det}\widetilde{K},$$

so $\log \text{Det}\widetilde{K} - \log \text{Det}\widehat{K} = \text{tr}(\widetilde{K}\widehat{K}^+) - (d-1) - 2D_{\text{KL}}^\perp(\widehat{K} \parallel \widetilde{K})$. Since $\widehat{K}\widehat{K}^+ = P$ is the projector onto $\mathbf{1}^\perp$, $\text{tr}(\widehat{K}\widehat{K}^+) = d-1$ and $\text{tr}(\widetilde{K}\widehat{K}^+) - (d-1) = \text{tr}((\widetilde{K} - \widehat{K})\widehat{K}^+)$. Substituting into $\ell(\widetilde{K}; T) - \ell(\widehat{K}; T) = (\log \text{Det}\widetilde{K} - \log \text{Det}\widehat{K}) - \text{tr}((\widetilde{K} - \widehat{K})T)$ gives

$$\ell(\widetilde{K}; T) - \ell(\widehat{K}; T) = -2D_{\text{KL}}^\perp(\widehat{K} \parallel \widetilde{K}) + \text{tr}((\widetilde{K} - \widehat{K})(\widehat{K}^+ - T)),$$

which is (11). The upper-side bound (12) follows by dropping the non-positive KL term and applying Lemma A.2 with $A = T - \widehat{K}^+$. For (13), combine Lemma A.1 ($0 \leq 2D_{\text{KL}}^\perp \leq (d-1)\varepsilon^2/(2(1-\varepsilon))$ for $\varepsilon \in (0, 1)$) with Lemma A.2. \square

A.3. Proofs for Section 4. The Hüsler–Reiss Bregman identity (16) and the bound (17) are immediate from Theorem 3.1 under the substitution of Section 4.1.

Proof of Theorem 4.1. On $\mathbf{1}^\perp$ both Laplacians are positive definite. The spectral approximation (15) together with operator-monotonicity of the inverse on positive definite operators give $\Theta^+/(1+\varepsilon) \preceq \widetilde{\Theta}^+ \preceq \Theta^+/(1-\varepsilon)$ on $\mathbf{1}^\perp$. For each pair $i \neq j$, the vector $b_{ij} := e_i - e_j$ lies in $\mathbf{1}^\perp$, so $\widetilde{\Gamma}_{ij} = b_{ij}^\top \widetilde{\Theta}^+ b_{ij}$ inherits the two-sided bound, giving (18). The same argument applies to any pair, so all variogram entries are preserved multiplicatively. \square

Proof of Corollary 4.2. Let $v(y) := \binom{y}{1} \in \mathbb{R}^{d+1}$. By the Hüsler–Reiss density representation (6),

$$\log \lambda_{\widetilde{\Theta}}(y) - \log \lambda_{\Theta}(y) = -\frac{1}{2}(\log |\det \widetilde{C}| - \log |\det C|) - \frac{1}{2}v(y)^\top (\widetilde{C}^{-1} - C^{-1})v(y).$$

Step 1 (Cayley–Menger perturbation). The Cayley–Menger blocks yield $\widetilde{C} - C = \begin{pmatrix} -(\widetilde{\Gamma} - \Gamma)/2 & 0 \\ 0 & 0 \end{pmatrix}$, so $\|\widetilde{C} - C\|_2 = \frac{1}{2}\|\widetilde{\Gamma} - \Gamma\|_2$. The two-sided bound (18) of Theorem 4.1 reads $\Gamma_{ij}/(1+\varepsilon) \leq \widetilde{\Gamma}_{ij} \leq \Gamma_{ij}/(1-\varepsilon)$, which translates to the entrywise bound $|\widetilde{\Gamma}_{ij} - \Gamma_{ij}| \leq \frac{\varepsilon}{1-\varepsilon}\Gamma_{ij}$ (the upper deviation $\varepsilon/(1-\varepsilon)$ dominates the lower $\varepsilon/(1+\varepsilon)$). Since Γ has nonnegative entries, monotonicity of the spectral radius on nonnegative matrices (Wielandt’s theorem) gives $\rho(|\widetilde{\Gamma} - \Gamma|) \leq \frac{\varepsilon}{1-\varepsilon}\rho(\Gamma)$, and the symmetry of both matrices together with $\|A\|_2 \leq \rho(|A|)$ for symmetric A gives $\|\widetilde{\Gamma} - \Gamma\|_2 \leq \rho(|\widetilde{\Gamma} - \Gamma|) \leq \frac{\varepsilon}{1-\varepsilon}\|\Gamma\|_2$. Hence $\|\widetilde{C} - C\|_2 \leq \eta_C$. Using $\|\Gamma\|_2$ here, instead of the entrywise Frobenius bound $\|\widetilde{\Gamma} - \Gamma\|_F \leq \frac{\varepsilon}{1-\varepsilon}\|\Gamma\|_F$ that an entry-by-entry summation would give, saves up to a factor of \sqrt{d} for generic variograms.

Step 2 (log-determinant and inverse perturbation). Write $M_\Theta := \|C^{-1}\|_{\text{op}} = 1/s_{\min}(C)$, so $s_i(C) \geq s_{\min}(C) = 1/M_\Theta$ for every i . Assuming $\eta_C M_\Theta < 1$, Weyl’s inequality for singular values ($|s_i(\widetilde{C}) - s_i(C)| \leq \|\widetilde{C} - C\|_2 \leq \eta_C$) gives

$$s_i(\widetilde{C}) \geq s_i(C) - \eta_C \geq 1/M_\Theta - \eta_C = (1 - \eta_C M_\Theta)/M_\Theta > 0 \quad \text{for every } i,$$

and, writing $t_i := s_i(\widetilde{C})/s_i(C) - 1$, $|t_i| \leq \eta_C/s_i(C) \leq \eta_C M_\Theta < 1$. Using $|\log(1+t)| \leq |t|/(1-|t|)$ for $|t| < 1$ (immediate from $\log(1+t) = \int_0^1 t/(1+\tau t) d\tau$), each term satisfies $|\log(s_i(\widetilde{C})/s_i(C))| = |\log(1+t_i)| \leq |t_i|/(1-|t_i|) \leq \eta_C M_\Theta/(1-\eta_C M_\Theta)$. Summing over the $d+1$ singular values of C ,

$$\begin{aligned} |\log |\det \widetilde{C}| - \log |\det C|| &= \left| \sum_{i=1}^{d+1} \log(s_i(\widetilde{C})/s_i(C)) \right| \\ &\leq \sum_{i=1}^{d+1} |\log(1+t_i)| \leq (d+1)\eta_C M_\Theta/(1-\eta_C M_\Theta), \end{aligned}$$

where the first equality uses $|\det A| = \prod_i s_i(A)$. For the inverse perturbation, the resolvent identity $\tilde{C}^{-1} - C^{-1} = C^{-1}(C - \tilde{C})\tilde{C}^{-1}$ together with $\|C^{-1}\|_2 = M_\Theta$ and $\|\tilde{C}^{-1}\|_2 = 1/s_{\min}(\tilde{C}) \leq M_\Theta/(1 - \eta_C M_\Theta)$ gives

$$\|\tilde{C}^{-1} - C^{-1}\|_2 \leq M_\Theta \cdot \eta_C \cdot M_\Theta / (1 - \eta_C M_\Theta) = \eta_C M_\Theta^2 / (1 - \eta_C M_\Theta),$$

whence $|v^\top (\tilde{C}^{-1} - C^{-1})v| \leq \|v\|_2^2 \|\tilde{C}^{-1} - C^{-1}\|_2 = (\|y\|_2^2 + 1) \eta_C M_\Theta^2 / (1 - \eta_C M_\Theta)$ (using $\|v(y)\|_2^2 = \|y\|_2^2 + 1$). Combining the two bounds yields (20). The block bound $M_\Theta \leq \|\Theta\|_{\text{op}} + \|p\|_2 + |\sigma^2|$ in (19) follows by triangle inequality on the three-block decomposition $\text{CM}(\Gamma)^{-1} = \text{diag}(\Theta, 0) + \begin{pmatrix} 0 & p \\ p^\top & 0 \end{pmatrix} + \text{diag}(0, \sigma^2)$, whose summands have operator norms $\|\Theta\|_{\text{op}}$, $\|p\|_2$, and $|\sigma^2|$. The sample-mean bound (21) follows by averaging the pointwise bound over Y_1, \dots, Y_n . \square

APPENDIX B. TUNING-PARAMETER SWEEPS FOR THE DANUBE EXPERIMENT

(a) Spectral-HR (η)				(b) eglearn-NS (ρ)				(c) eglearn-glasso (ρ)			
η	Edges	BIC	AIC	ρ	Edges	BIC	AIC	ρ	Edges	BIC	AIC
1.10	31	1,521.17	1,435.52	0.005	364	2,012.63	1,007.19	0.005	291	1,694.26	890.46
1.20	33	1,364.65	1,273.51	0.014	184	1,342.91	834.65	0.044	171	1,342.77	870.42
1.30	34	1,342.50	1,248.57	0.023	130	1,179.36	820.27	0.083	151	1,419.73	1,002.66
1.50	35	1,304.76	1,208.03	0.032	99	1,176.96	903.52	0.123	146	1,531.34	1,128.08
2.00	38	1,285.98	1,181.02	0.041	89	1,281.88	1,036.02	0.162	160	1,538.49	1,096.53
2.50	39	1,281.27	1,173.57	0.050	82	1,309.73	1,083.25	0.201	167	1,556.78	1,095.49
3.00	42	1,284.30	1,168.24	0.091	56	1,519.46	1,364.76	0.240	174	1,577.94	1,097.32
4.00	46	1,264.47	1,137.42	≥ 0.132	—	—	—	0.279	171	1,571.67	1,099.38
5.00	46	1,264.51	1,137.36					0.319	170	1,543.69	1,074.12
6.00	48	1,268.55	1,135.94					0.358	170	1,558.03	1,088.46
8.00	48	1,268.56	1,135.97					0.397	162	1,566.80	1,119.37
10.00	48	1,268.54	1,135.96					0.436	158	1,544.02	1,107.65
15.00	50	1,265.87	1,127.77					0.476	150	1,567.54	1,153.21
20.00	52	1,268.46	1,124.90					0.515	134	1,561.81	1,191.68
25.00	53	1,268.75	1,122.36					0.554	128	1,709.41	1,355.88
30.00	53	1,268.76	1,122.35					0.593	117	1,707.47	1,384.33
40.00	55	1,277.55	1,125.62					≥ 0.632	—	—	—
50.00	56	1,281.89	1,127.23								
75.00	57	1,287.81	1,130.40								
100.00	60	1,302.26	1,136.53								

TABLE 4. Full tuning-parameter sweeps on the Danube data for the three tunable methods: edge count, BIC and AIC (22) at every grid point. (a) Spectral-HR over the BSS parameter η , (b) eglearn-NS over the ℓ_1 parameter ρ , (c) eglearn-glasso over ρ . Bold marks the parameter selected by each criterion. Rows listed as “—” (in (b) for $\rho \geq 0.132$ and in (c) for $\rho \geq 0.632$) correspond to grid points where the estimated graph is disconnected and $\hat{\Gamma}$ cannot be completed.

DEPARTMENT OF MATHEMATICS AND COMPUTER SCIENCE, EINDHOVEN UNIVERSITY OF TECHNOLOGY, EINDHOVEN, THE NETHERLANDS

Email address: i.echave.sustaeta.rodriquez@tue.nl

DEPARTMENT OF MATHEMATICS AND COMPUTER SCIENCE, EINDHOVEN UNIVERSITY OF TECHNOLOGY, EINDHOVEN, THE NETHERLANDS

Email address: a.abiad@tue.nl

DEPARTMENT OF APPLIED MATHEMATICS, UNIVERSITY OF TWENTE, ENSCHEDE, THE NETHERLANDS

Email address: f.rottger@utwente.nl